



CHAPTER 1

Introduction and motivation

”Le silence éternel de ces espaces infinis m’effraie”, Blaise Pascal in les pensées 206, fragment 91.

1.1 Probing the universe

1.1.1 Short historical background and discovery of the interstellar medium

Already Claude Ptolemy (90-168) described our galaxy as ”a zone as white as milk“ [Ferrière, 2001]¹ and in the 5th century BC, Demokrit believed that the Milky Way consists of a countless number of stars [Steinmetz, 2012]. Indeed this is a remarkable guess, knowing well that Demokrit did not have a modern instrument, like a telescope equipped with state-of-the-art hardware, which he could use to test his theory. In 1610, Galileo Galilei (1564-1642) was the first person who observed the Milky Way through an optical telescope and he saw innumerable dim stars. Moreover, together with Johannes Kepler (1571-1630) he reached to the common conclusion of the heliocentric movement of the planets which can be seen as the first study of the dynamics of astronomical objects. About one century earlier, this behavior of the planets has been proposed by Nikolaus Copernicus (1473-1543). Isaac Newton (1643-1727) benefited from the research of Galilei and Kepler and could complete their observations with his equations of motion which together with today’s gravitation theory can explain the complicated movement of planets. Not until the 18th century it became clear that our galaxy appears as a flat disk in which the earth and our planetary system is deeply embedded. Eventually, at the end of the 18th century it was William Herschel (1738-1822) who performed a systematic study of the star distribution across the sky. However, Herschel erroneously concluded that the galaxy is about five times more extended in the galactic plane than in its perpendicular direction and that the sun is located near the galactic center. A supplemental work to Herschel’s was conducted by Jacobus Kapteyn (1851-1922) and he found a spatial distribution of stars in our galaxy having exponential scale lengths at half maxi-

¹Further historical facts on pages 1-3 are taken from the same reference except when otherwise cited.



mum of 1.2 kpc in the radial and 0.22 kpc in the vertical direction²(new results give 3.5 kpc and 0.25 kpc obtained from the RAVE experiment [Steinmetz et al., 2006]). Herschel and Kapteyn assumed that all stars have approximately the same intrinsic brightness and that the interstellar space is completely transparent to starlight, therefore, completely neglecting the obscuring interstellar matter between the stars. On the other hand, Edward Barnard (1857-1923) revealed on his astronomical photographs that in the Milky Way there are many dark zones with various shapes and sizes. Soon after it was realized that these dark regions might be due to clouds of interstellar matter hiding the stars behind them. This argument was supported by Hartmann's discovery (1904) of stationary absorption lines of Ca^+ in the spectrum of the spectroscopic binary δ -Orionis which could only have an interstellar origin.

Another component of the interstellar medium (ISM) is dust which was concluded by Trumpler (1930) on the basis of the observed reddening effect which lets light emitted by faraway stars appear to us redder than it actually is. The reason for this effect is that shorter wavelength blue light is more effectively scattered by dust grains of comparable size. Large scale magnetic fields are another component of the ISM and align dust particles in the direction of the magnetic field, resulting in a linear polarization of starlight [Davis and Greenstein, 1951].

The third basic constituent of the ISM are cosmic rays originating from magnetobremstrahlung mainly from relativistic electrons. This source of radiation was identified by Ginzburg and Syrovatskii [1965]³ during their explanation of the galactic radio emission.

Shortly after Hartmann's discovery of gaseous phases in the ISM, during World War I, Harlow Shapley (1885-1972) took another approach to estimate our position in the galaxy and observed that globular clusters concentrate in the direction of the Sagittarius constellation having roughly a spherical distribution with the center being approximately the center of our galaxy. Shapley radically concluded that our sun lies very far from the galactic center at a distance of about 15 kpc away, a distance overestimation of a factor 2 as became clear in later years. In the 1920s, Bertil Lindblad (1895-1965) and Jan Oort's (1900-1992) kinematic studies of the relative velocities of stars and globular clusters with respect to the sun showed the validity of their differentially rotating galactic model with the sun at a distance previously predicted by Shapley, whereas the relative velocities were difficult to match to the total amount of mass predicted by Kapteyn's model. After a suggestion of van de Hulst [van de Hulst, 1945] and along with the invention of microwave devices, measurements of the spatial distribution of neutral hydrogen became possible [Ewen and Purcell, 1951; Muller and Oort, 1951]. Their measurements proofed that Shapley was correct about the off-center position of the sun and that its galactocentric radius was overestimated by a factor 2. Compared to earlier measurements of visible starlight, the measurement of the non-visible 21 cm radio-emission of neutral hydrogen is a truly pioneering experiment. In

²1 kpc = 1000 pc = 3260 light years = $3.09 \cdot 10^{16}$ km

³Later Ginzburg was awarded the Nobel prize in physics in the field of condensed matter theory/superconductivity.

the following centuries, the success of this measurement motivated the development of instruments sensitive to even shorter non-visible wavelengths, such as the submillimeter (submm) regime which approximately spans the frequencies from 0.3-3 THz. Radiation in this wavelength regime contains important informations about the star-forming process.

Nowadays, we know that our galaxy consists of a thin disk with a radius of approximately 25-30 kpc and an effective thickness of about 400-600 pc. The spherical system around the galactic center consists of a bulge with an approximate radius of 2-3 kpc and a galactic halo having an extension of 30 kpc from the center. The sun is embedded in the disk about 15 pc above the mid plane and 8.5 kpc away from the galactic center [references within Ferrière, 2001].

Astronomy is one of the oldest sciences but even today there is no clear answer to current questions how stars form and how galaxies, like our own, form and evolve [Freeman and Bland-Hawthorn, 2002]. Furthermore, seemingly trivial questions about the mass of e.g. extragalactic nebulae [Zwicky, 1937] are difficult to answer because of the so-called missing mass problem. This problem is probably universal since also in our own galaxy it is observed that the mean velocity of stars circulating around the galactic center only weakly depends on the galactocentric radius [Brand and Blitz, 1993]. The observed exponential decrease of the mass density with aforementioned scale lengths should result in a slower velocity, however, a constant velocity of about 220 km/s is measured.

1.1.2 Interstellar molecules, chemical networks and star formation - Tracers and spectral resolution

Stars are formed during the collapse of gravitationally unstable molecular clouds of the ISM. A collapse can only occur when the gravitational force is larger than the internal pressure p of the molecular gas (Jeans criterion)

$$\frac{\partial p}{\partial r} \leq -G \frac{\rho M(r)}{r^2} . \quad (1.1)$$

Here, ρ is the mass density of the cloud, $M(r)$ is the total mass inside a given radius r and G is the gravitational constant.

In order to obtain a detailed understanding of star formation, it is important to resolve the various physical processes inside a molecular cloud. Molecular level transitions inside a cloud result in the emission of electromagnetic waves with frequencies in the submm frequency band or are due to the absorption of continuum photons by the surrounding molecular gas or dust, providing the possibility to measure and understand the process of star formation. For these studies it turns out that the submm frequency band contains approximately half of the total luminosity of the Universe and almost all (98%) photons which were emitted since the Big Bang [Blain et al., 2002]. However, these processes are difficult to quantify since the dust makes the clouds opaque to visible or infrared light. Moreover, the emitted waves with submm wavelengths lie in the non-

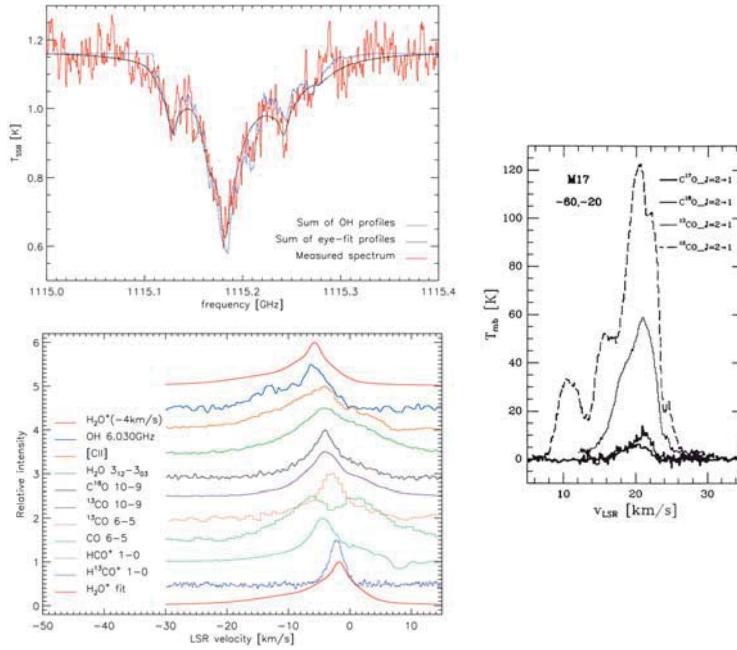


Figure 1.1: Left top: Hyperfine multiplet resolved H_2O^+ molecular line in the massive star forming region DR21 from Ossenkopf et al. [2010] observed with the HIFI instrument on the HERSCHEL space observatory [de Graauw et al., 2010]. Left bottom: Comparison of the velocity structure of various chemical tracers in DR21 taken from Ossenkopf et al. [2010]. Right: Observation of isotopic CO $J = 2 \rightarrow 1$ transitions in the Messier 17 molecular cloud core from Stutzki and Güsten [1990] using the IRAM 30 m telescope on Pico Veleta, Spain. This measurement resolves complex emission line features, the low-dip features are due to self-absorption of surrounding gas.

visible part of the electromagnetic spectrum which necessitates adapted detection techniques.

The key technology needed to explore the physics of the ISM, this means to obtain as much as possible informations from observations of interstellar molecules through their emission or absorption lines, are state-of-the-art receivers equipped with the most sensitive detectors providing a very high spectral resolution and intermediate-frequency bandwidth. This technology has to be combined with telescopes having a minimum rms dish surface-roughness of the order of 10-20 μm and a low-loss optical beam-path.

A distant galaxy rotates with a typical velocity of $v_{\text{rot}} = 10^2$ km/s. The result is that the observed emission line of a molecule inside the galaxy will be broadened due to the Doppler effect by $\Delta\nu = 2\nu \cdot v_{\text{rot}}/c$, with ν being the observed frequency from the molecule (which might be additionally Doppler shifted due to a relative motion of the source to the observer). For example, for $\nu = 1$ THz, the width of a molecular line is approximately $\Delta\nu = 1$ GHz and a large intermediate-frequency bandwidth is needed to measure the complete molecular line. Nearby galaxies like the Large Magellan Cloud show very narrow spectral lines of order 10 km/s where the fundamental reason for the linewidth is due to magnetohydrodynamic turbulences in the cloud. In order to resolve molecular lines here, this necessitates not only a wide intermediate frequency bandwidth but also a spectral resolution

of order 10^4 . Figure 1.1 shows three examples in which the need for a very high spectral resolution is even more evident. For example, the measurement of the H_2O^+ hyperfine multiplet requires an instrument with a spectral resolution of at least 10^5 - 10^6 and to resolve the velocity profile of this emission line requires a resolution of about 0.1 km/s or better. A comparable velocity resolution rendered the measurement of Stutzki and Güsten [1990] possible and they observed complex self-absorption features in the velocity profile of the isotopic CO $J = 2 \rightarrow 1$ transitions towards Messier 17.

A high spectral resolution instrument, however, needs a sufficient high sensitivity in order to fulfill the requirements of state-of-the-art astronomical experiments, examples are given in the next section. Nowadays, instruments use two different types of detectors. Frequency mixers which sense radiation coherently and direct detectors which measure the power of the radiation field without intermediate-frequency mixing step. Coherent or heterodyne detection instruments used in submm terahertz astronomy make use of superconductor-insulator-superconductor (SIS) mixers up to frequencies of 1.4 THz and receivers for frequencies above 1.4 THz employ hot-electron bolometer mixers (HEB) [Zmuidzinas and Richards, 2004]. Direct detection instruments which are employed in the 1 THz frequency regime, generally use either mature technology transition edge sensors (TES) like e.g. described by Goldie et al. [2011] or a new type of direct detector called microwave kinetic-inductance detector (MKID) [Day et al., 2003]. The next section first compares recent and future observational experiments at KOSMA before section 1.2 compares the advantages and the disadvantages of coherent and direct detection techniques, their fundamental sensitivity limits and the requirements for their applicability in astronomical observations.

1.1.3 Comparison of recent and future observational experiments and receiver developments at KOSMA - Need for array compatible heterodyne detectors at 1 THz

The “Kölner Observatorium für Submillimeter Astronomie” (KOSMA) at the “I. Physikalisches Institut of the Universität zu Köln” has a long-established tradition in combining observational astronomy research and detector device research. New observations, for example at increasingly higher frequencies or where very high sensitivities are needed, often require new detector concepts or a reconsideration of materials combinations (chapters 3 - 7 of this thesis).

Figure 1.2 shows two telescopes which are the target instruments for the detector technologies developed in this thesis. Below I give a brief summary about the recent and future detector developments of our group and how they are completed by observations with the example of the future observatory CCAT.

The recent detector developments at KOSMA, e.g. for band 2 of the HIFI instrument [de Graauw et al., 2010] on the Herschel space observatory or for the 1.4, 1.9 and 2.5 THz modular dual-color heterodyne instrument GREAT [Pütz et al., 2012; Heyminck et al., 2012] on the Stratospheric Observatory for



Figure 1.2: Left: Atacama Pathfinder Experiment (APEX) telescope on 5107 m altitude on Llano de Chajnantor in the Chilean High Andes [Güsten et al., 2006]. Right: Design study of the Cerro Chajnantor Atacama Telescope (CCAT) how it should look like when its constructional work is finished in 2020. The planned telescope site is on a plateau on 5612 m altitude just below Cerro Chajnantor with worldwide unparalleled weather conditions [CCAT 2011].

Infrared Astronomy (SOFIA), showed state-of-the-art performance and enabled very successful observations.⁴ Usually, these single-ended detector designs are made for single-pixel operation, although small arrays of these detectors can be practically realized in a receiver like e.g. in SMART or CHAMP⁺.

Nowadays the quantum-limited operation of simple single-ended SIS mixers (compare with figure 1.5) in astronomical receivers, at least up to 700 GHz, is a mature technique. Furthermore, it is not foreseeable if research on hot-electron bolometric mixer devices will result in a significant sensitivity improvement in the near future. It is, therefore, evident that astronomical receivers with single-pixel detectors reached already their sensitivity limit. However, a further significant improvement in the sensitivity can be achieved by employing detector arrays, i.e. a large number of very sensitive detectors which can observe several positions in the sky simultaneously and use the sparse observation time at a telescope more efficient than a single-pixel detector.

One of the worldwide very few heterodyne detector arrays is operated from KOSMA at the NANTEN 2 telescope at 4865 m altitude on Pampa la Bola in the Atacama desert, Chile. Here a dual color 492/806 GHz heterodyne receiver (SMART, Sub-Millimeter Array Receiver for Two Frequencies) with 8 pixels per frequency is successfully operated since several years.

A further important improvement of astronomical observations with the goal to find new physics of the ISM, is to increase the angular resolution θ of a telescope. The diffraction limit of a telescope follows the well-known Rayleigh criterion $\sin \theta \approx \theta = 1.22 \cdot \lambda/D$, with D being the aperture of the telescope and λ the wavelength of the observed light. The consequence on the observation time of high angular-resolution surveys compared to already existing observations can be summarized with the help of table 1.1. The table compares four observatories with each other, from which some of them are supposed to implement arrays of

⁴Early science results from SOFIA observations are contained in the Astronomy&Astrophysics special issue vol. 542, June 2012.

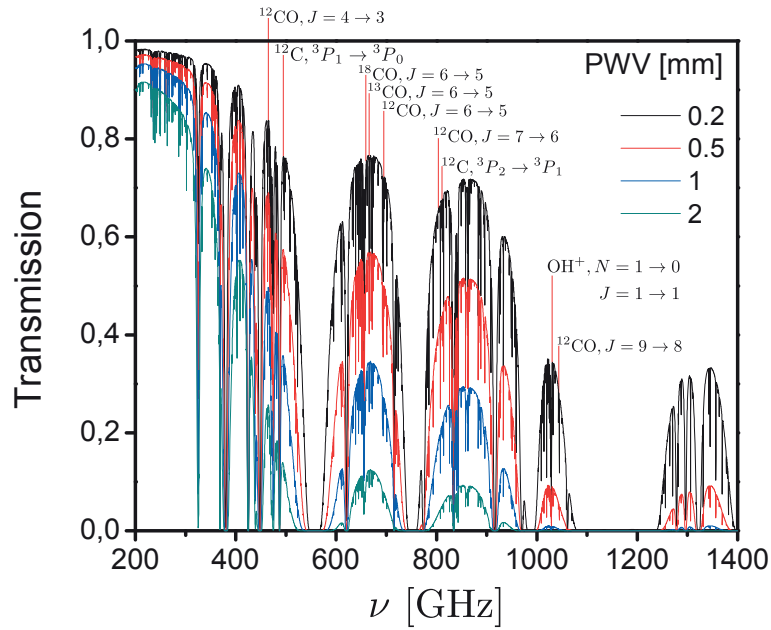


Figure 1.3: Simulated atmospheric transmissivity [APEX2010] of submm frequencies at the APEX site on Llano de Chajnantor for four different PWV values of 0.2 mm, 0.5 mm, 1 mm and 2 mm. A selection of some important stellar molecules, considered as important for CCAT as noted by Goldsmith [2011], is shown illustrating the difficulty of ground-based astronomical observations due to atmospheric absorption. Frequencies within the gap between approximately 1.1 THz and 1.25 THz, where e.g. a molecular transition of the important chemical tracer H_2O^+ can be observed, cannot be sensed from ground-based observatories but from airborne or space space observatories (compare with figure 1.1).

heterodyne mixers. At $\lambda = 610 \mu\text{m}$, the telescopes APEX and NANTEN 2, due to the difference in the aperture, differ in their angular resolution by approximately a factor three. CCAT will have a better angular resolution by a factor of two compared to APEX and by a factor of approximately five to NANTEN 2. It will be mainly used to observe extended astronomical sources. Due to its large focal-plane area, CCAT is an ideal heterodyne mapping-instrument, i.e. which can be used for continuum surveys and spectroscopic mapping. Principally, complementary observations with the Atacama Large Millimeter Array (ALMA) [Wootten and Thompson, 2009] are possible which has the largest angular resolution among all telescopes in the world due to its kilometer-long baseline. However, here the scientific goals are different.

The CCAT site has worldwide unparalleled weather conditions which result in the highest atmospheric transparency in the world and in the possibility to observe nearly all important tracers from the ground like indicated in figure 1.3. With the complementary observations of CCAT and ALMA it will be possible to resolve molecular cloud structures with unprecedented quality by using already observed molecular lines as tracers like the low- J CO transitions. The scientific motivation of these extensive observations is that it is very likely that astrochem-

Table 1.1: Comparison of four observatories in terms of their angular resolution and survey time evaluated at $\lambda = 610 \mu\text{m}$ ($^{12}\text{C}, ^3\text{P}_1 \rightarrow ^3\text{P}_0$) for CCAT, APEX and NANTEN 2 and at $\lambda = 158 \mu\text{m}$ ($\text{C}^+, ^2\text{P}_{3/2} \rightarrow ^2\text{P}_{1/2}$) for SOFIA. $\Omega_b \propto \theta^2$ denotes the solid angle of the antenna beam [Rohlfs and Wilson, 1999]. The time t_{surv} estimates the observation time for a large scale survey ($\Omega_{\text{surv}} = (1^\circ)^2$) for $\varepsilon = 0.5$ and for the parameter sets shown in table 1.2. The present GREAT receiver on SOFIA is not a mapping instrument and the survey time for this instrument is only included for a relative comparison to the survey times of the other instruments.

		CCAT	APEX	NANTEN 2	SOFIA
D [m]		25	12	4	2.7
θ [arcsec]		6	13	38	15
Ω_b [arcmin ²]		0.011	0.053	0.45	0.071
t_{surv} [s]	# 1	$6.5 \cdot 10^7$	$1.4 \cdot 10^7$	$1.6 \cdot 10^6$	—
	# 2	$1.6 \cdot 10^7$	$3.4 \cdot 10^6$	$4.0 \cdot 10^5$	—
	# 3	$2.0 \cdot 10^6$	$4.2 \cdot 10^5$	$5.0 \cdot 10^4$	—
	# 4	$5.5 \cdot 10^5$	—	—	—
	# 5	$1.4 \cdot 10^5$	—	—	—
	# 6	$3.4 \cdot 10^4$	—	—	—
	# 7	—	—	—	$1.6 \cdot 10^8$

Table 1.2: Collection of parameter sets used to calculate t_{surv} in table 1.1 using eq. (1.3). The value for $\Delta\nu$ corresponds to a moderate velocity resolution of approximately 0.5 km/s at a wavelength of $\lambda = 610 \mu\text{m}$ and 0.2 km/s at a wavelength of $\lambda = 158 \mu\text{m}$. The single-sideband receiver noise-temperatures are average values which can be achieved with SIS mixers coupled to a telescope beam, i.e. including the atmospheric contribution to the noise temperature.

#	$T_{\text{rec}}^{\text{SSB}}$ [K]	$\Delta\nu_{\text{ch}}$ [MHz]	ΔT [K]	N_p
1	1000	1	0.1	1
2	500	1	0.1	1
3	500	1	0.1	8
4	1000	1	0.1	120
5	500	1	0.1	120
6	500	1	0.1	480
7	4000	1	0.1	1

istry and the molecular cloud structure are crucial for the evolution of a molecular cloud. This can only be resolved by high-angular resolution instruments.

Detector arrays significantly improve the observation efficiency. A straightforward estimation of the survey time as a function of the array size shows the great

potential of these instruments like for example discussed by Goldsmith [2011]. Assuming proper Nyquist sampling and a final image with angular resolution equal to θ (table 1.1), the ratio of the solid angle of the survey to the solid angle of the antenna beam, Ω_{surv}/Ω_b , can be expressed as

$$\frac{\Omega_{surv}}{\Omega_b} = N_p t_{surv} \varepsilon \Delta\nu_{ch} \left(\frac{\Delta T}{T_{rec}^{SSB}} \right)^2, \quad (1.2)$$

which results in the total time for a survey

$$t_{surv} = \frac{\Omega_{surv}}{\Omega_b} \left(\frac{T_{rec}^{SSB}}{\Delta T} \right)^2 \frac{1}{\varepsilon \Delta\nu_{ch} N_p}. \quad (1.3)$$

In the above formulas, T_{rec}^{SSB} is the single-sideband receiver noise-temperature, ΔT is the temperature resolution which one would like to achieve and $\Delta\nu_{ch}$ is the spectrometer's intermediate-frequency channel bandwidth. Further details are given in section 1.2.1 and figure 1.4. The mapping efficiency ε depends on the time for calibrating the telescope, slewing, telescope acceleration, etc., and N_p is the number of detectors in the array.

Table 1.1 summarizes the time t_{surv} needed for a survey with $\Omega_{surv} = (1^\circ)^2 = 3600^2$ for four different observatories. Due to the large focal plane of CCAT, this telescope allows to operate a larger array than for example APEX or NANTEN 2. Presently, SOFIA is not used as a mapping instrument, however, in the near future the upGREAT instrument will be commissioned and will provide observations on SOFIA with a small heterodyne array of HEB mixers. The survey time given in table 1.1 for SOFIA is thus an unfair comparison, however, it quantifies the difference between the instruments as of now. For example, with an array of 120 detectors, CCAT can survey a solid angle of $(1^\circ)^2$ three times faster and with a twice as large resolution than APEX could do that with an array of 8 detectors. Nonetheless, for the detector development in this thesis, APEX and NANTEN 2 are very important platforms since they provide the possibility to test small array concepts which have a technological impact on the detector array development for CCAT.

Arrays of detectors are not only used for large scale mapping as described above. They have a second important aspect when they are used in the terahertz frequency regime. Here they are needed to efficiently use the sparse observation time which is a difficult task because of the changing weather conditions. In these circumstances an array of detectors is employed to e.g. spatially resolve nearby galaxies with a single-shot read-out of the detector signal.

In order to conclude this section, the text below discusses a major disadvantage of the array concept realized in the SMART receiver operated at NANTEN 2. The discussion below has had a major impact on the detector technologies studied in this thesis. In particular, SMART is not easily scalable to significantly more than sixteen pixels, mainly due to the following reasons:

1. The distribution of the reference frequency radiation (compare with section 1.2.1) to the individual mixers is achieved using a Fourier grating [Graf and Heyminck, 2001]. Due to the low output power of THz LO sources, this approach limits the maximum number of the pixels one can achieve in an heterodyne array.
2. Nowadays, synthesizer-driven local-oscillator sources (SLO's) are being used as reference-frequency sources over a large part of the terahertz frequency regime up to approximately 3 THz due to their easy operation. Chapter 6 of this thesis describes a method which quantifies the noise contribution of a SLO. We find that the equivalent noise contribution for present SLO devices is comparable to the receiver sensitivity. This noise contribution, therefore, degrades the performance of a conventional multi-pixel array usually using a single-ended mixer technology. In order to fully exploit the advantage of a many-pixel heterodyne array it is necessary to use a mixer technology which is not sensitive to the noise coming from the SLO, like balanced mixers [Kooi et al., 2012; Westig et al., 2011; Serizawa et al., 2008; Maas, 1986].
3. A third major disadvantage is that the sky signal and the reference frequency are superimposed using optical diplexing. For many pixels this is usually achieved with Martin-Puplet or Fabry-Pérot interferometers which lead to two major disadvantages. First, this way of combining two signals works only over a certain bandwidth and limits the instantaneous intermediate-frequency (IF) bandwidth of the heterodyne receiver system. Second, the complexity of the interferometer increases with the pixel number and eventually large interferometers are needed in multi-pixel heterodyne receivers which increase the system complexity.

These reasons justify to reconsider how sky signal and reference-frequency radiation can be superimposed in a more efficient way which does not limit the IF bandwidth, does not increase the system complexity and to suggest a technology most suitable for arrays of detectors.

1.2 Photon detectors for radio astronomy - Arrays and fundamental sensitivity

1.2.1 Coherent and incoherent detection

Coherent and incoherent photon detectors differ in their detection principle and the maximum sensitivity they can achieve. While incoherent detectors cooled to milli-Kelvin temperatures where phonon noise (temperature fluctuations), noise from amplifiers and/or thermal loading and *Johnson-Nyquist* (white) noise are negligible, are ultimately only limited by photon-fluctuation noise, coherent detectors are fundamentally sensitivity limited due to the *Heisenberg* uncertainty

principle, even at milli-Kelvin temperatures. This section shortly summarizes the advantages and disadvantages of these two types of detectors with respect to an array configuration.

An upcoming trend in radio-astronomical terahertz instrumentation is to realize a technology very similar to what already has been realized in visual and infrared astronomy using CCD cameras. Incoherent terahertz detectors consist of simple circuitry. This is in particular the case for the MKID [Day et al., 2003] where additional simplicity is provided by the fact that most of the read-out circuitry is operated at room temperature. A very elegant frequency-domain multiplexing technique was already demonstrated where only two microwave ports are needed to read-out hundreds of these devices. It seems that the realization of a large array is quite feasible where pixel numbers of 1000 or even 10000 will be realized for future astronomical instruments where only intermediate spectral resolution is needed. On the other hand, high spectral resolution of a signal is difficult to achieve in a receiver which uses incoherent detectors. For example, a spectral resolution of 10^5 - 10^6 at a wavelength of $300 \mu\text{m}$ necessitates a 30-300 m grating spectrometer in-front of such an array. From a practical point-of-view such a system is clearly not possible.

Fabry-Pérot interferometers only transmit a limited bandwidth of frequencies, hence, they have a disadvantage in sensitivity when combined with a direct-detector array since they throw away photons and have to be scanned in order to obtain a complete frequency-spectrum.

Coherent receivers like the one shown in figure 1.4 easily achieve very high spectral-resolution due to the heterodyne technique. The central element of a heterodyne instrument is a mixer which shows a strong nonlinear current-voltage (I-V) characteristic (compare with figure 1.5). The high-frequency sky signal ν_{RF} in the range 0.3-3 THz is down-converted to frequencies in the total IF bandwidth $\Delta\nu_{IF}$ of the receiver in the frequency mixing device (detector) which produces the beat frequency between a reference signal (local oscillator, LO) with frequency ν_{LO} and the sky signal (RF). Intermediate frequencies are practically in the 4-20 GHz range. Among higher order terms and for a double-sideband receiver $\nu_{IF} = |\nu_{RF} - \nu_{LO}|$. Commercially available backend electronics, like cryogenic low-noise amplifiers and spectrometers are used to further process the IF signal. The typical channel bandwidth $\Delta\nu_{ch}$ of a high-resolution IF backend spectrometer is of order 100 kHz. Consequently, a 4 GHz IF signal can be resolved with a spectral resolution of order 10^5 due to the frequency down-conversion process of the high-frequency RF signal. It is difficult to put a large array of coherent detectors into practice, since e.g. in a SIS detector a magnetic field is needed to suppress the *Josephson* effect and the detector circuitry is more complex compared to incoherent devices. It consists of several microwave circuit-elements like impedance transformers, transmission-line transitions and different materials. For example, detector designs make use of combinations of different superconducting materials, hybrid structures including also normal conducting metals and various dielectric materials used for example as detector substrates or isolating circuit elements. This complexity has to be compensated by smart technologies to realize at least

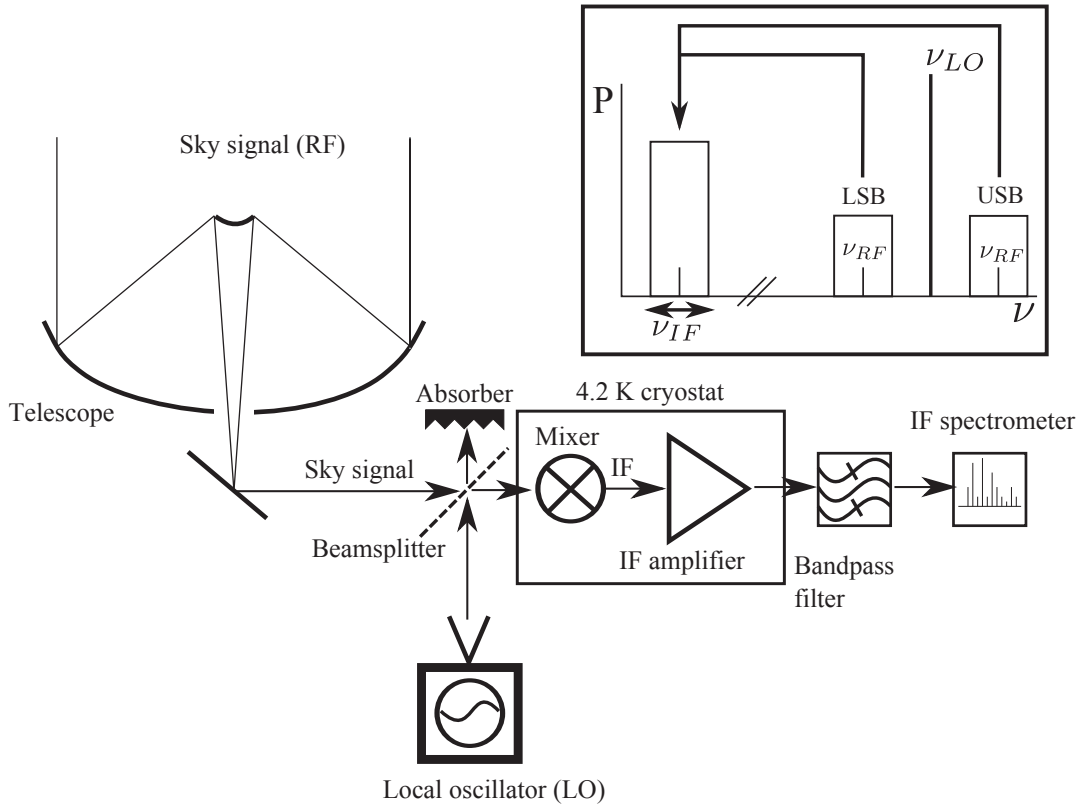


Figure 1.4: Sketch of a conventional double-sideband single-pixel heterodyne setup. The inset in the top right shows the down-conversion scheme. The two sidebands (LSB = lower sideband, USB = upper sideband) contain the desired (signal) frequency ν_{RF} . The LO carrier frequency is a strong continuous-wave line symmetrically between the upper and the lower sideband. In a double-sideband receiver during the downconversion process, both sidebands are convolved into the intermediate-frequency band with width $\Delta\nu_{IF}$. The IF spectrometer resolves the measured spectrum down to its channel bandwidth $\Delta\nu_{ch}$. Usually, LO and sky signal are superimposed inside a diplexer within a limited bandwidth and are then fed into the mixer device. When a beamsplitter is used instead of a diplexer (shown schematically in this figure), it does not limit the IF bandwidth, but in this case a LO is needed having a high output power.

a medium size array of for example 100 SIS detectors in the near future in our laboratory.

For a single-pixel receiver consisting of one incoherent detector, a measure for the sensitivity is the noise-equivalent power (NEP). It is defined as the signal power at the input of a detector which is necessary to produce a signal-to-noise ratio of unity at the output of the detector in $\Delta\nu = 1$ Hz detection bandwidth and is measured in units of $W/\sqrt{\text{Hz}}$ through the voltage noise and the responsivity. An incoherent detector is a device which measures power through sensing the square of the amplitude of the electromagnetic field. In the detection process there is no principle sensitivity limit, however, along with noise sources contained in the detector system itself, the sensitivity is limited due to photon fluctuations of the

thermal background. Assuming that no noise source is present, a measurement with a second detector attached at the output of the incoherent detector would measure exactly 0 W per unit bandwidth.

The sensitivity of a single-pixel coherent receiver consisting of one coherent detector is usually expressed in terms of an equivalent input noise-temperature T_{rec} . The measurement of this quantity uses the standard Y -factor method [Rohlf and Wilson, 1999]. Dependent on whether only one sideband or two sidebands are included in the characterization of the receiver, T_{rec} is defined as the single-sideband receiver noise-temperature and is denoted with the symbol T_{rec}^{SSB} or is defined as the double-sideband receiver noise-temperature and is denoted with the symbol T_{rec}^{DSB} . In order to circumvent difficulties in the definition of the receiver noise-temperature due to quantum mechanics, it is beneficial to define this quantity not as an equivalent temperature of a resistor but as follows: The receiver noise-temperature T_{rec} is equal to a temperature given by the exchangeable input noise-power per Hertz of a radiation source divided by the Boltzmann constant which, coupled to the input of a noiseless but otherwise identical receiver, gives the same output noise-power density as that of the actual receiver connected to a radiation source at absolute zero temperature [compare with remarks in Kerr, 1999]. An application of this definition is given in this thesis in section 2.1 in the framework of the fluctuation-dissipation theorem from which a first-principles derivation of the detector sensitivities is obtained. T_{rec} can be decomposed into the single noise contributions coming from each element in the receiver,

$$T_{rec} = T_1 + \frac{T_2}{G_1} + \frac{T_3}{G_1 G_2} + \dots = T_1 + \sum_{i=2}^n \frac{T_i}{\prod_{j=1}^{i-1} G_j} . \quad (1.4)$$

The variables T_i and G_i are the equivalent noise temperatures and gains of each element shown in figure 1.4. After an integration time τ the minimum detectable temperature is equal to [Stutzki, 2007; Rohlf and Wilson, 1999]

$$\Delta T = \frac{T_{rec}}{\sqrt{\tau \Delta \nu_{IF}}} , \quad (1.5)$$

where $\Delta \nu_{IF}$ is the intermediate-frequency (IF) bandwidth. A comparison between NEP and T_{rec} is provided by the relation

$$NEP = k_B T_{rec} \sqrt{\Delta \nu_{IF}} , \quad (1.6)$$

where a factor "2" has to be included when T_{rec} is measured in a single-sideband receiver. When the output noise-power equals the input noise-power, $T_{rec} = 0$. Particularly this result is never possible when using a coherent detector since this device amplifies at least the vacuum fluctuation of the electromagnetic field into the classical regime where it is finally measured, provided that the detector is phase insensitive, i.e. measures equally the amplitude and the phase of a signal. In fact the following statement always holds. The minimum output noise-temperature referred to the input of a coherent receiver is equal to $h\nu/k_B$

(≈ 47 K/THz, quantum limit) like derived in section 2.1 of this thesis in the framework of the fluctuation-dissipation theorem. This is the fundamental explanation for the sensitivity limit observed during the characterization of the detectors developed in this thesis (compare with chapter 5).

In contrast to these detectors, for an incoherent detector, the vacuum energy of the electromagnetic field does not represent an exchangeable energy and cannot be measured, therefore, does not represent a sensitivity limit [Clerk et al., 2010; Gavish et al., 2000], also shown in section 2.1. This result is once more obtained theoretically in appendix A.2.2 on the basis of a two-level system (electron in a magnetic field), modeling the incoherent detector. Here we can highlight unambiguously the fundamental difference between the detection modes when using an incoherent and on the other hand a coherent detector.

1.2.2 Superconductive waveguide mixers on silicon membranes

Circuit elements with a strong nonlinear current-voltage (I-V) characteristic can be used in radio-frequency (RF) circuits as frequency mixers and are implemented in heterodyne receivers in order to provide coherent detection of signals with high spectral resolution (figure 1.4). For submm frequencies, nowadays two common frequency mixers are Nb/ AlO_x /Nb or high current-density Nb/ AlN /Nb [Kawamura et al., 2000; Zijlstra et al., 2007] superconductor-insulator-superconductor (SIS) contacts and thin (≈ 4 nm) superconducting films which are the most important elements in hot-electron bolometer mixers (HEBs). SIS receivers were first reported in the 1979's [Richards et al., 1979; Dolan et al., 1979]. Nowadays, SIS device research focusses on increasing the detection frequency together with achieving the highest sensitivity [Zmuidzinas and Richards, 2004].

The first reported bolometer mixers were made of the semiconducting material InSb in a balanced-mixer configuration [Phillips and Jefferts, 1973]. In these devices, instead of the strong nonlinear I-V characteristic of a superconducting thin-film microbridge (HEB), the nonlinear I-V characteristic of the InSb material was used for heterodyne mixing. On the other hand, state-of-the-art superconducting HEB detectors use films of either NbTiN or NbN superconductors [Pütz et al., 2012], however, their functionality is not restricted to these materials only. Bevilacqua et al. [2012] shows a measured performance of a HEB detector at 600 GHz of 600 K by using a MgB_2 film. The motivation of using MgB_2 films or other high-gap superconducting materials is to overcome the decreased IF bandwidth of HEB mixers (0-3 GHz) which represents a major limitation in radio-astronomical observations and molecular line surveys. In contrast to that is the wide IF bandwidth of SIS mixers which practically covers the frequencies 0-20 GHz and is only limited by technical challenges like the design of broadband IF circuitry. The text below compares SIS and HEB mixer technologies with respect to their applicability to heterodyne arrays of detectors.

At KOSMA, the traditional mixer technology are waveguide mixers, mainly motivated by the needs of the optical setups in radio telescopes. The first optical

element of these heterodyne mixers are waveguide horn-antennas which provide a well defined Gaussian beam. This beam is coupled efficiently to the telescope optics. On the device side, the horn antenna is attached to a rectangular full-height waveguide shown in figures 1.5(a) and (b). The device antenna extends into this waveguide and picks up the signals which are then coupled to the mixing device via a tuning circuit. A major difficulty of fabricating waveguide mixer-blocks in which the mixer circuits are embedded are the filigree mechanical structures often only a few hundred microns large.

In the past, traditional mixer circuits were fabricated on quartz (SiO_2) substrates which had to be glued into a tellurium-copper waveguide mixer-block. Since the thickness of the substrate limits the performance at higher frequencies, quartz substrates had to be polished down to provide mixer operation also at terahertz frequencies. This additional step in the mixer fabrication constitutes a risk since the substrate can break, it is time consuming and most importantly the thickness which can be achieved is limited by the structure of the quartz. A good yield is achieved for substrate thicknesses of the order of 20-40 μm , but below this value the probability is high to destroy the circuit by breaking the substrate. A further disadvantage is that between the mixer block and the substrate a mismatch in the thermal conductance can occur, which might lead to heat trapping in the device with the result of a decreased performance. From a microwave point of view, mixers using quartz substrates glued directly into the mixer block have a larger capacitive coupling and due to this reason cannot provide large IF bandwidths.

All these disadvantages are solved by the silicon (Si) or silicon nitride (SiN) membrane technology in combination with the beam-lead process first reported by Kaul et al. [2004] and reviewed by Zmuidzinas and Richards [2004] in the framework of superconducting mixers. A bulk handle wafer consists of a thick Si layer, followed by a SiO layer used as an etch stop in the microfabrication process of the mixers and the Si device layer consisting of a high-resistivity membrane available in various thicknesses, for example ranging from 3-12 μm . SiN wafers are available with membranes which are e.g. only 1-2 μm thick.

After fabrication of the mixer circuit, the device is mounted into a waveguide mixer-block by ultrasonic bonding on the beam-lead contacts. Since the beam-lead contacts hold the device suspended in the waveguide, the capacitive coupling to the ground potential is minimal and this allows circuit designs with a large IF bandwidth as reported by Kaul et al. [2004]. Furthermore, it is assumed that there is no thermal boundary between mixer block and the superconducting device, because the beam-lead material is gold and should, therefore, provide a good thermal contact to the tellurium-copper material of the mixer block. This assumption is supported by experimental results. For example, in figure 1.5(e) the superconducting gap energy of a mixer device using two Nb/ AlO_x /Nb SIS junctions in a series circuit shows the expected value for 4.2 K bath temperature of $2 \cdot (\Delta_1 + \Delta_2) / e = 5.6 \text{ mV}$, even with applied LO radiation, i.e. with input of energy. Here $2\Delta_{1,2}$ are the superconducting pair-breaking energies of the respective SIS electrodes, also called superconducting gap-energies.